EphA2 Affects Development of the Eye Lens Nucleus and the Gradient of Refractive Index

Catherine Cheng,[1] Kehao Wang,[2] Masato Hoshino,[3] Kentaro Uesugi,[3] Naoto Yagi,[3] and Barbara Pierscionek[4]

[1]School of Optometry, Indiana University, Bloomington, IN, United States
[2]Beijing Advanced Innovation Centre for Biomedical Engineering, Key Laboratory for Biomechanics and Mechanobiology of Ministry of Education, School of Engineering Medicine, Beihang University, Beijing, China
[3]Japan Synchrotron Radiation Research Institute (Spring-8), 1-1-1, Kouto, Sayo-cho, Sayo-gun, Hyogo 679-5198 Japan
[4]Faculty of Health, Education, Medicine and Social Care, Medical Technology Research Centre, Anglia Ruskin University, Chelmsford Campus, United Kingdom

Correspondence: Catherine Cheng, Indiana University, School of Optometry, 800 E. Atwater Ave., Bloomington, IN 47405, USA; ckcheng@iu.edu.

Received: November 1, 2021
Accepted: December 13, 2021
Published: January 3, 2022

Citation: Cheng C, Wang K, Hoshino M, Uesugi K, Yagi N, Pierscionek B. EphA2 affects development of the eye lens nucleus and the gradient of refractive index. *Invest Ophthalmol Vis Sci.* 2022;63(1):2. https://doi.org/10.1167/iovs.63.1.2

Purpose. Our studies in mouse eye lenses demonstrate that ephrin-A5 and EphA2 are needed for normal epithelial cells and lens transparency. We sought to determine whether EphA2 and ephrin-A5 are important for lens morphometrics, nucleus formation, and refractive index.

Methods. We performed tissue morphometric measurements, electron microscopy, Western blots, and interferometric measurements using an X-ray synchrotron beam source to measure the gradient of refractive index (GRIN) to compare mouse lenses with genetic disruption of EphA2 or ephrin-A5.

Results. Morphometric analysis revealed that although there is no change in the overall lens volume, there is a change in lens shape in both *EphA2*$^{-/-}$ lenses and *ephrin-A5*$^{-/-}$ lenses. Surprisingly, *EphA2*$^{-/-}$ lenses had small and soft lens nuclei different from hard lens nuclei of control lenses. SEM images revealed changes in cell morphology of *EphA2*$^{-/-}$ fiber cells close to the center of the lens. Inner *EphA2*$^{-/-}$ lens fibers had more pronounced tongue-and-groove interdigitations and formed globular membrane morphology only in the deepest layers of the lens nucleus. We did not observe nuclear defects in *ephrin-A5*$^{-/-}$ lenses. There was an overall decrease in magnitude of refractive index across *EphA2*$^{-/-}$ lenses, which is most pronounced in the nucleus.

Conclusions. This work reveals that Eph-ephrin signaling plays a role in fiber cell maturation, nuclear compaction, and lens shape. Loss of EphA2 disrupts the nuclear compaction resulting in a small lens nucleus. Our data suggest that Eph-ephrin signaling may be required for fiber cell membrane reorganization and compaction and for establishing a normal GRIN.

Keywords: GRIN, interdigitation, fiber cells, SEM, ephrin-A5

The eye lens is composed of a monolayer of epithelial cells on the anterior hemisphere, and the bulk of the lens is made up of elongated fiber cells. Lifelong lens growth depends on the proliferation, differentiation, and elongation of epithelial cells at the lens equator into newly fiber cells.[1] Layers of differentiating fiber cells elongate and surround the previous shell of lens fibers.[2,3] During fiber cell differentiation, cytoplasmic organelles and nuclei are lost to eliminate light scattering structures in mature fiber cells in the lens core.[4] In mammalian lenses, it is thought that lens fiber cells at the center, or nucleus, of the lens may become compacted.[5,6] However, lens nucleus compaction does not occur in all species,[7,8] and the mechanism requires elucidation.

Fine focusing of light images onto the retina requires a highly refractive, transparent and avascular lens that changes shape to focus light from near and far objects, in a process known as accommodation. Age-related changes in lens stiffness and elasticity lead to an inability of the lens to change shape during accommodation, leading to a condition called presbyopia and a need for reading glasses.[5,9–13] Increased lens stiffness with age has been reported in humans[5,13–21] and animal models,[21–23] including mice,[24–29] and stiffening of aging human lenses has been hypothesized to be caused by increased nucleus size and stiffness with age.[5,30] Our recent study demonstrated that mouse lenses increase in stiffness and nuclear size throughout life.[29] It has long been hypothesized the increase in nuclear size and density with age may be linked to both age-related nuclear cataracts and presbyopia.[5,6,30–32] However, the mechanism for nuclear growth and increase in density throughout life is unknown, and the link between nuclear size, overall lens stiffness, and maintenance of transparency is unclear.

Recent reports have shown that disruptions of EphA2 or ephrin-A5 in humans and mice lead to cataracts,[33–48] defined as any lens opacity. Eph receptors are the largest

class of receptor tyrosine kinases, and bidirectional signaling is mediated by the binding of Eph receptors to membrane-anchored ephrin ligand. This signaling pathway is involved in tissue development and plays key roles in cell-cell contact, adhesion, repulsion, and migration.[49-52] The Eph-bearing cell experiences forward signaling whereas the ephrin-bearing cell undergoes reverse signaling.[53,54] There are 14 Eph receptors, divided into EphA (1 to 8 and 10) and EphB (1 to 4 and 6) classes, and there are eight ligands classified as ephrin-A (1 to 5) and ephrin-B (1 to 3). Each ligand and receptor can have multiple binding partners. EphA2 mutations cause human congenital dominant[41,43,47,48,55,56] and recessive cataracts,[42] and non-synonymous SNPs in EphA2 and ephrin-A5 genes have been linked to human age-related cataracts.[33,34,36,39,40,46,56] In mice, loss of EphA2 is associated with disruption of the actin cytoskeleton, cell shape and organization of equatorial epithelial cells,[44] and with misaligned and disorganized fiber cells.[33,37,38,44,57] Changes in refractive index[37] and an increased stress response reflected by elevated Hsp27 levels have also been reported in EphA2 knockout (*EphA2*$^{-/-}$) lenses.[33] In contrast, *ephrin-A5*$^{-/-}$ mouse lenses in the C57BL6 background often develop anterior cataracts due to epithelial-mesenchymal-transition knockout (KO) anterior epithelial cells.[38]

With mounting evidence that Eph-ephrin signaling is required for lens homeostasis, we investigated the role of EphA2 and ephrin-A5 in lens morphology, nuclear and gradient refractive index (GRIN) formation. Both *EphA2*$^{-/-}$ and *ephrin-A5*$^{-/-}$ lenses are more spherical than littermate controls. Surprisingly, loss of EphA2 leads to a much smaller lens nucleus and nuclear fibers with abnormal fiber cell membrane interdigitations. There is a significant decrease in the magnitude of the refractive index in the *EphA2*$^{-/-}$ lens nucleus. Although *ephrin-A5*$^{-/-}$ lenses had normal lens nuclei, there are small defects in nuclear fiber cell morphology and a small decrease in the maximum refractive index in the *ephrin-A5*$^{-/-}$ lens nucleus. Our data suggest that EphA2 and ephrin-A5 are needed for normal lens shape and that EphA2 is essential for normal nuclear fiber cell membrane interdigitations and fiber cell maturation.

Material and Methods

Mice

Mice were maintained in accordance with an approved animal protocol (Indiana University Bloomington Institutional Animal Care and Use Committee) and the ARVO Statement for the Use of Animals in Ophthalmic and Vision Research. Generation of *Ephrin-A5*$^{-/-}$ and *EphA2*$^{-/-}$ mice was previously described.[38,44,58,59] Automated qPCR on toe or tail snips were used for genotyping (Transnetyx, Cordova, TN, USA). Genotyping confirmed that all mice were wild-type *Bfsp2* (CP49) genes, and mice were maintained in the C57BL/6J strain background. Male and female littermates were used for experiments.

Lens Morphometrics

Morphometrics of freshly dissected eight-week-old control and KO lenses was obtained in 1X DPBS at room temperature as previously described.[24,25,28] Eight lenses from four mice of each genotype were used for these experiments. Briefly, lenses were photographed under a dissection microscope using a right-angle mirror, and lens nuclei were isolated from decapsulated lenses by gentle rolling the lens between gloved fingertips to remove soft cortical fibers. The nucleus is much stiffer than the surrounding cortical fibers in mouse lenses.[25,28,29] The exceptions were the *EphA2*$^{-/-}$ lens nuclei that were much softer. Cortical fibers from *EphA2*$^{-/-}$ lenses were removed using the method for isolating nuclei for protein extraction outlined below. FIJI software was used to perform image analysis, and Excel and GraphPad Prism 9 were used to calculate and plot lens volume (volume = $4/3 \times \pi \times r_E^2 \times r_A$, where r_E is the equatorial radius and r_A is the axial radius), lens aspect ratio (ratio between axial and equatorial diameters), nuclear volume (volume = $4/3 \times \pi \times r_{Ne}^2 \times r_{Na}$ where r_{Ne} is the equatorial radius of the lens nucleus and $\times r_{Na}$ is the axial radius of the lens nucleus), nuclear fraction (ratio between the nuclear volume and the lens volume), and nuclear ration (ratio between nuclear axial and nuclear equatorial diameters). Plots represent mean ± standard deviation. Student *t*-tests between KO lenses and their respective controls were used to determine statistical significance.

To remove the lens cortex via vortexing, we used the same method as described below for protein extraction. At least eight lenses from four mice of each genotype were used for these experiments. For the eight-week-old lenses, the decapsulated fiber cell mass was vortexed for four minutes in 30 second pulses to completely remove cortical fiber cells. Lens nuclei were inspected and photographed in clean 1X Dulbecco's phosphate-buffered saline (DPBS) after removal of the lens cortex. Nuclear size and shape from *EphA2*$^{+/+}$ lenses were not statistically different between the mechanical and vortexing methods for lens cortex removal.

Scanning Electron Microscopy

Lenses from eight-week-old control and KO mice were prepared for scanning electron microscopy (SEM) using a protocol that was adapted from previous work.[60-62] A small hole was made in the posterior of freshly enucleated eyes. Eyeballs were fixed in freshly made and oxygenated fixative buffer (2.5% glutaraldehyde in 0.1M sodium cacodylate buffer, pH 7.3) at room temperature for 72 hours. Lenses were then dissected from eyes in fixative buffer warmed to 37°C, and each lens was fractured using a sharp razor blade along the visual axis. This orientation exposes interlocking protrusions and paddles along the short sides of fiber cells. Lens halves were placed in fresh fixative buffer for 72 hours at room temperature. Samples were washed in 0.1M sodium cacodylate buffer for three times and 10 minutes per wash. Lens halves were post-fixed in 1% aqueous OsO_4 for 90 minutes at room temperature and then washed in ddH_2O three times for 10 minutes per wash. Samples were then dehydrated using ethanol (50%, 70%, 70%, 95%, 95%, 100%, and 100%) for 30 minutes per step and then dried overnight in an Autosamdri 815 critical point dryer (Tousimis, Rockville, MD, USA). Lens halves were mounted and sputter coated with iridium (10 mA current thickness of 5.8–6.0 nm) with an EMS Q150T S sputter coater. Images were acquired with a Hitachi S4800 scanning electron microscope (Hitachi, Tokyo, Japan) 5 kV. Sequential images were collected from the center of the sample toward the periphery along the equatorial axis. Images were analyzed after lining up sequential images from the center to the periphery to ensures regions were comparable. Six

lenses from 3 different mice of each genotype were examined, and representative images are shown in Results.

X-Ray Talbot Interferometry

X-ray Talbot interferometry was performed as previously described at the SPring-8 facility (Japan).[29,63-65] Eight-week-old eyes from control and KO mice were stored in Dulbecco's modified Eagle medium without phenol red (21063–029; ThermoFisher, Carlsbad, CA, USA) with 2% penicillin/streptomycin (15-140-122, ThermoFisher) at room temperature before experiments. At least six eyes from each genotype were analyzed. Matlab (2020a, MathWorks, Natick, MA, USA) was used to calculate the refractive index from X-ray Talbot interferometry measurements to generate two-dimensional (2D) iso-indicial index contours and three-dimensional (3D) meshed index profiles in the mid-sagittal plane (anterior-posterior plane through the visual axis) of each mouse eye and mid-coronal plane (cross section view) of each mouse lens through the center of the lens. GRIN profiles were generated along the visual axis by Matlab, and the means and standard deviations were calculated in Excel and plotted in GraphPad Prism 9. Student's *t*-test or Welch's test between KO and respective control samples were used to determine statistical significance.

Lens Protein Extraction and WES Capillary-Based Immunoassay

Fresh lenses from six-week-old mice were collected and stored at −80°C until homogenization. Two lenses from each mouse were pooled into one protein sample. At least three pairs of lenses of each genotype were used to make separate protein samples. For whole lens samples, lenses were homogenized on ice in a glass Dounce homogenizer in 250 µL of lens homogenization buffer (20 mM Tris-HCl pH 7.4 at 4°C, 100 mM NaCl, 1 mM $MgCl_2$, 2 mM EGTA and 10 mM NaF with 1 mM DTT, 1:100 Protease Inhibitor Cocktail [P8430, Sigma-Aldrich, St. Louis, MO, USA] and one tablet of Pierce Phosphatase Inhibitor Mini Tablets per 10 mL buffer [A32957, ThermoFisher] added on the day of the experiment) per 10 mg of lens wet weight. Homogenized whole lens proteins were transferred to a new Eppendorf tube and briefly sonicated. Whole lens proteins were diluted 1:1 with 2X sample buffer (0.21M Tris-HCl [pH 6.8], 2.86 mM ethylenediamine tetra-acetic ETDA, 21% sucrose, 6.67% SDS, and 0.3M DTT in ddH_2O) and stored at −20°C until use.

For epithelial cell, cortical fiber and nuclear fiber protein fractions, freshly isolated lenses were immediately processed after dissection. Lens epithelial cells adhere strongly to the capsule.[38,66] To isolate epithelial cells, whole lenses were gently ruptured at the lens equator, and whole capsules were gently removed and placed in lens homogenization buffer (14.75 µL for two lens capsules from the same mouse). Lens epithelial cell extract was mixed with 1.25 µL of 2X sample buffer and further mixed by pipetting through a P10 pipette tip. Two fiber cell masses from the same mouse were then moved an Eppendorf tube containing 250µl of 1:1 lens homogenization buffer and 2X sample buffer. Fiber cell masses were vortexed at top speed for 30 second pulses four times. Visual inspection after vortexing showed softer outer cortical fibers were completely removed, leaving the lens nuclei, which were the expected size based on comparison to morphometric experiments. The hard lens nuclei were carefully removed with clean tweezers from the cortical fiber cell protein lysate to a glass Dounce homogenizer with 250 µL of 1:1 lens homogenization buffer and 2X sample buffer. Homogenized nuclear protein samples were then collected into a clean Eppendorf tube. Fiber cell protein samples were briefly sonicated, and all samples were stored at −20°C until use.

Protein concentration were quantified using Quick Start Bradford Protein Assay (Bio-Rad, Hercules, CA, USA) using manufacturer instructions and measured by nanodrop. Equal amounts of control and KO proteins for each fraction (whole lens, epithelial cells, cortical fibers and nuclear fibers) were prepared based on manufacturer instructions for loading into a capillary-based (Western [WES]) immunoassay using a 12-230kDa Separation module kit according to the manufacturer's instructions (ProteinSimple, San Jose, CA, USA). Antibodies and protein concentrations were previously titrated to determine the range for antibody saturation and linear concentrations of protein extracts. To detect EphA2 protein levels, 3mg/mL of whole lens, cortical fiber or nuclear protein extract were loaded onto WES plates and probed with rabbit anti-EphA2 antibody (1:50, 6997; Cell Signaling Technology, Danvers, MA, USA). Epithelial cell samples had much lower protein concentrations than samples from other parts of the lens, and 0.2 mg/mL of epithelial cell proteins were used for EphA2 WES experiments. Loading control was determined by total protein detected using a Total Protein Separation module kit (ProteinSimple). WES data was detected as chemiluminescent peaks in a capillary presented in electropherogram format, and a pseudo-lane view, akin to a traditional Western blot, is also shown. Protein level calculations were determined by calculating the area under the peak from the EphA2 signal (128 kDa) and normalizing that to the area under all of the peaks from the total protein assay. Average and standard deviations were calculated in Excel, and normalized protein amounts and representative electropherograms were plotted in GraphPad 9. Student's *t*-test between KO and respective control samples were used to determine statistical significance.

Results

EphA2$^{-/-}$ Lenses Have Smaller Nuclei With Lower Magnitude of Refractive Index

To better understand the roles of EphA2 and ephrin-A5 in the lens, we conducted detailed morphometric measurements, including lens and nuclear volume, as well as lens and nuclear shape (i.e., aspect ratio), in eight-week-old control and KO lenses. We first examined control and *ephrin-A5*$^{-/-}$ lenses, and although there is no change in lens volume, nuclear volume and nucleus aspect ratio, *ephrin-A5*$^{-/-}$ lenses were slightly more spherical than control lenses and had a decrease in lens aspect ratio (Fig. 1A). When we measured *EphA2*$^{-/-}$ lenses, there was a similar decrease in lens aspect ratio when compared to controls, and *EphA2*$^{-/-}$ lenses have smaller lens nuclei with abnormal disc shape (Supplemental Fig. S1). In all our previous studies, mouse lens nuclei were rigid and incompressible bodies that were left after mechanical removal of the soft cortical fibers between gloved fingertips.[25,28,29,61,62] When using mechanical disruption to remove the lens cortex from the nucleus, *EphA2*$^{-/-}$ lens nuclei felt softer than those of control lenses. It is plausible that mechanical removal of cortical fibers may have damaged the softer lens nucleus

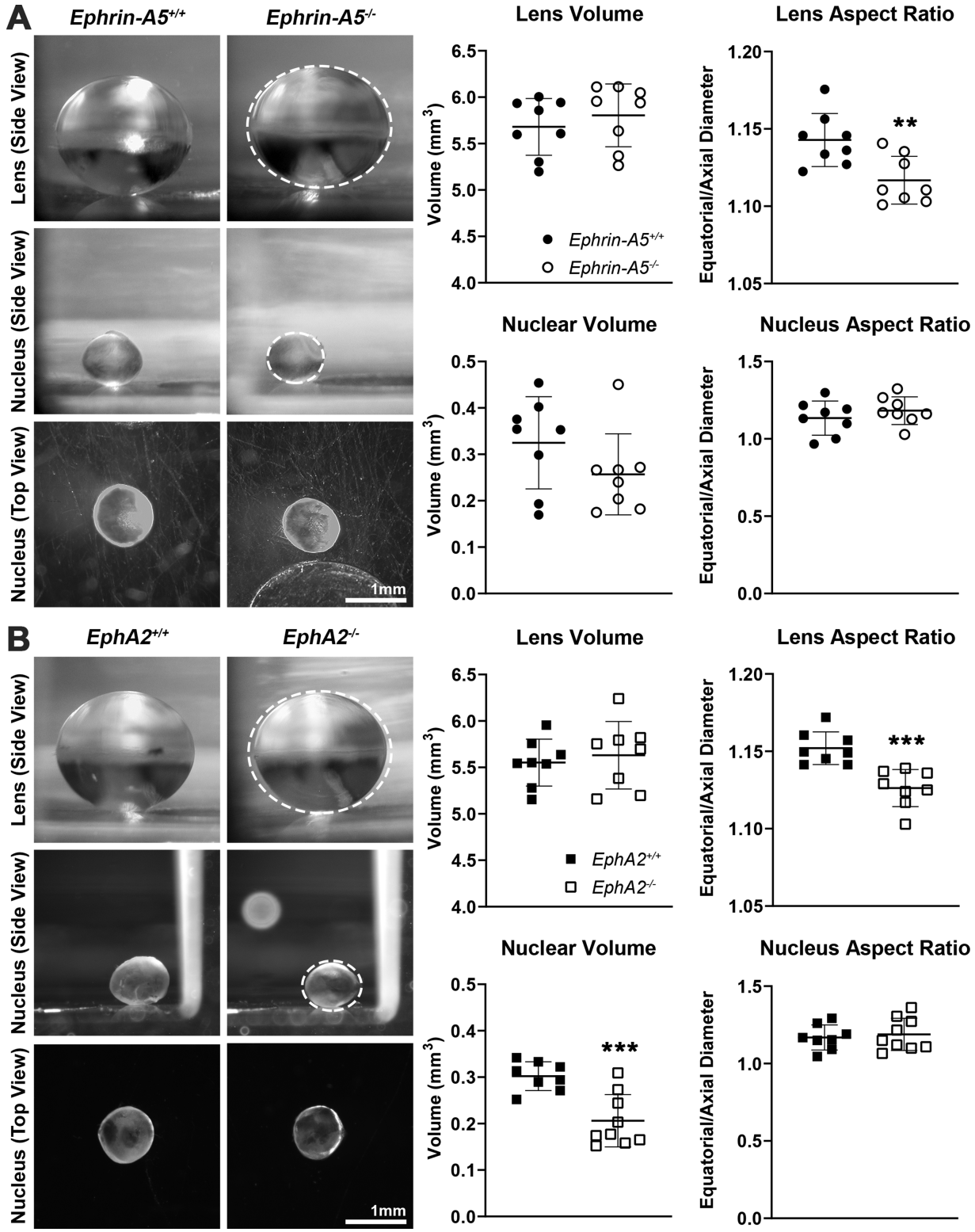

Figure 1. Morphometric measurements from 8-week-old control and KO lenses (n = 8 for each genotype). (**A**) Representative images of the lens (*side view*) and nucleus (*side* and *top views*) are shown for control and *ephrin-A5*$^{-/-}$ lenses. There is no significant change in lens volume, nuclear volume and nuclear shape (aspect ratio) between control and *ephrin-A5*$^{-/-}$ lenses. However, *ephrin-A5*$^{-/-}$ lenses are slightly more spherical with decreased lens aspect ratio. The *dotted ellipse* on the *ephrin-A5*$^{-/-}$ lens picture is an outline of the control lens, revealing a change in the *ephrin-A5*$^{-/-}$ lens shape. The *dotted ellipse* in the *ephrin-A5*$^{-/-}$ nucleus picture is an outline of the control nucleus, showing there is no change in nucleus size or shape. (**B**) Similarly, there was no significant change in lens volume between control and *EphA2*$^{-/-}$ lenses, but *EphA2*$^{-/-}$ lenses were rounder with decreased aspect ratio. The *dotted ellipse* on the *EphA2*$^{-/-}$ lens picture is an outline of the control lens to highlight the change in lens shape. *EphA2*$^{-/-}$ lens nuclei were smaller than those from control lenses. The *dotted ellipse* in the *EphA2*$^{-/-}$ nucleus picture is an outline of the control nucleus, demonstrating a significant decrease in nucleus size. All plots represent the average ± the standard deviation. *Scale bars*: 1 mm. **, $P < 0.01$; ***, $P < 0.001$; ****, $P < 0.0001$.

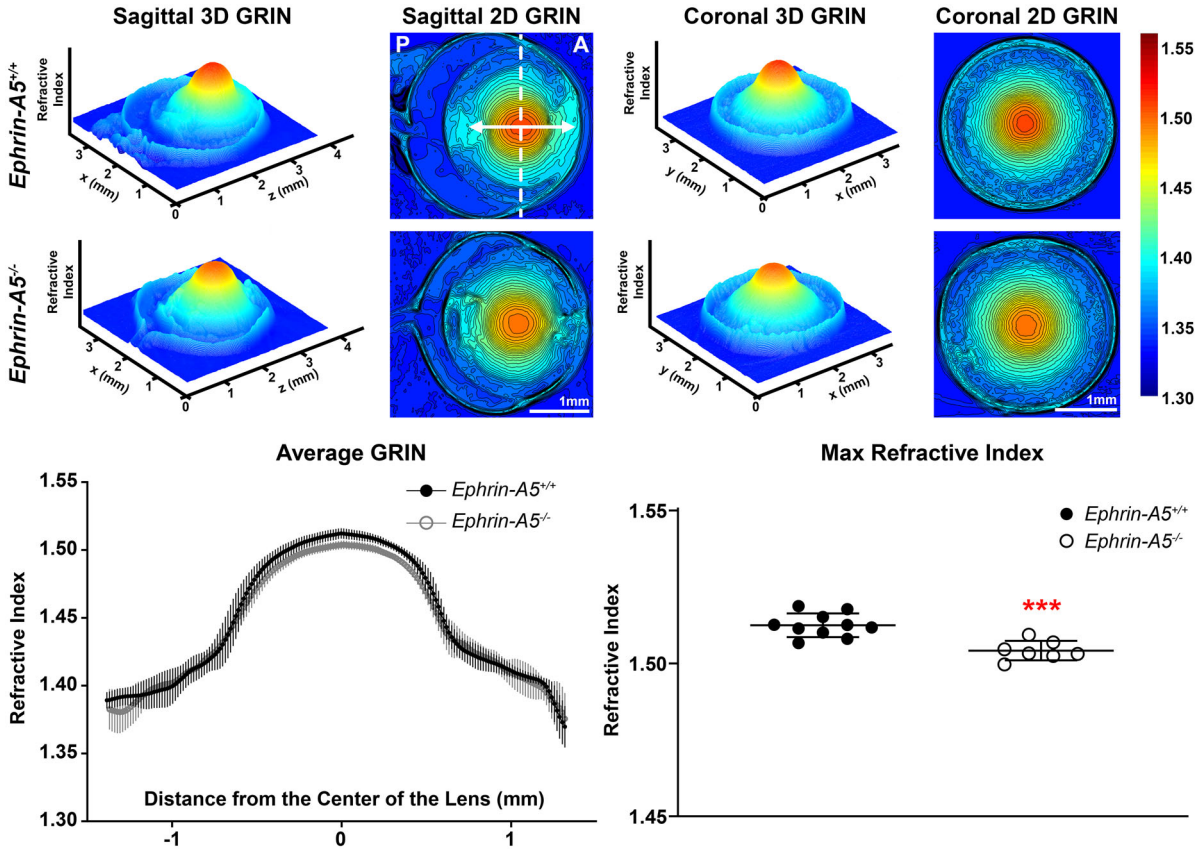

Figure 2. Gradient of refractive index (GRIN) 3D mesh and 2D contour plots of whole eyes from 8-week-old control and *ephrin-A5*$^{-/-}$ mice. 2D contour plots are shown through the mid-sagittal plane (anterior-posterior plane through the visual axis) and the mid-coronal plane (cross section view) passing through the center of the lens nucleus. The anterior (*A*) and posterior of the eye (*P*) are marked on the sagittal view of the control eye. The *dotted line* through the 2D sagittal view represents the location of the coronal 3D and 2D heat maps. A rainbow gradient of colors reflects the magnitude of refractive index from low refractive index in dark blue (1.30) to high refractive index in dark red (1.55). Control and *ephrin-A5*$^{-/-}$ lenses have comparable 3D and 2D GRIN plots. GRIN profiles from the lens along the visual axis were extracted, and the average and standard deviation are plotted for control (n = 10) vs. *ephrin-A5*$^{-/-}$ lenses (n = 7). The difference between control and *ephrin-A5*$^{-/-}$ GRIN profiles is not statistically significant. The maximum refractive index at the center of the lens is slightly decreased in *ephrin-A5*$^{-/-}$ lenses. Average GRIN and max refractive index plots represent the average ± the standard deviation. ***, $P < 0.001$.

of *EphA2*$^{-/-}$ lenses causing an unnatural shape change. Thus we used a vortexing method to remove the cortical fibers without applying compressive forces from *EphA2*$^{+/+}$ and *EphA2*$^{-/-}$ lenses. When comparing size and shape of nuclei in *EphA2*$^{+/+}$ lenses after mechanical or cortical removal by vortexing, there was no difference in the volume or aspect ratio between the two methods. Our data revealed that the volume of the *EphA2*$^{-/-}$ lens nuclei were smaller, but the nuclear shape (aspect ratio) was similar to that of control and *EphA2*$^{-/-}$ lenses (Fig. 1B). These results indicate that EphA2 is essential for development of lens nuclear size and may affect nuclear stiffness.

The area of highest refractive index in mouse lenses is closely correlated with the lens nucleus.[29] Thus we investigated whether the change in *EphA2*$^{-/-}$ lens nuclei affects the gradient refractive index (GRIN). We measured GRIN in control, *ephrin-A5*$^{-/-}$ and *EphA2*$^{-/-}$ lenses. In *ephrin-A5*$^{-/-}$ lenses, the GRIN profiles as shown in 3D heat maps and 2D profiles were similar to those of controls (Fig. 2). However, there was a small but statistically significant decrease in the maximum refractive index at the center of *ephrin-A5*$^{-/-}$ lenses when compared to that of controls. This result suggested that the *ephrin-A5*$^{-/-}$ lens nucleus may not be completely developed. GRIN measurements in *EphA2*$^{-/-}$ lenses showed a pronounced decrease across the entire lens, but this was most pronounced at the lens nucleus, when we compared the 3D heat maps and the 2D profiles along the visual axis (Fig. 3). There was a significant decrease in the maximum refractive index at the center of the *EphA2*$^{-/-}$ lens nucleus, indicating that the loss of EphA2 affected formation of the GRIN and linked to the under development of the nucleus.

Loss of EphA2 Affects Mature Fiber Cell Membrane Interdigitations

To determine the possible cause of changes in *EphA2*$^{-/-}$ lens nuclei, we performed scanning electron microscopy (SEM) to compare fiber cell morphologies between control, *ephrin-A5*$^{-/-}$ and *EphA2*$^{-/-}$ lenses. In control and *ephrin-A5*$^{-/-}$ lenses, we observed normal cortical fiber cells with small interlocking protrusions on the short sides and well-organized inner fiber cells with large paddles and protrusions on their short sides (Fig. 4A, panels 1-2). As the fiber cells continued to mature, cell membranes were relatively

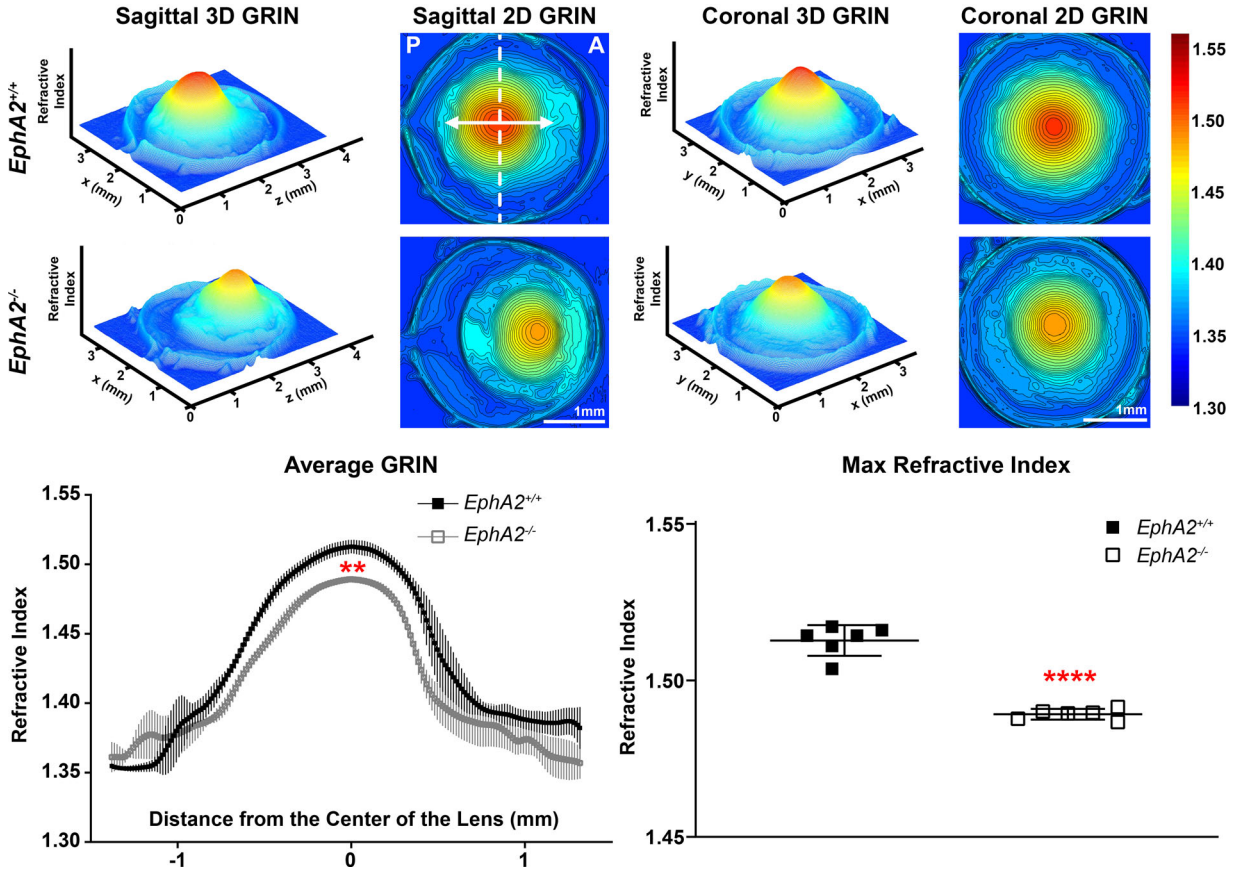

Figure 3. GRIN 3D mesh and 2D contour plots of whole eyes from 8-week-old control and *EphA2*$^{-/-}$ mice. 2D contour plots are shown through the mid-sagittal plane (anterior-posterior plane through the visual axis) and the mid-coronal plane (cross section view) passing through the center of the lens nucleus. The anterior (*A*) and posterior of the eye (*P*) are marked on the sagittal view of the control eye. The *dotted line* through the 2D sagittal view represents the location of the coronal 3D and 2D heat maps. A rainbow gradient of colors reflects the magnitude of refractive index from low refractive index in dark blue (1.30) to high refractive index in dark red (1.55). *EphA2*$^{-/-}$ lenses have obviously decreased GRIN when compared to control 3D and 2D plots. The central region of *EphA2*$^{-/-}$ lenses is orange, rather than deep red as seen in controls, indicating a lower refractive index in mutant compared to control lenses. *EphA2*$^{-/-}$ lenses (n = 6) had significantly decreased average GRIN profiles and max refractive index at the center of the lens when compared to controls (n = 6). Average GRIN and max refractive index plots represent the average ± the standard deviation. **, $P < 0.01$; ****, $P < 0.0001$.

smooth with large interlocking protrusions on the short side between cells (Fig. 4A, panels 3 and insets 3′, *arrowheads*), and there was the formation of tongue-and-groove interdigitations along the long sides of fiber cells, as well as in the large protrusions on the short sides of fiber cells (Fig. 4A, panels 4 and insets 4'). Perinuclear fiber cells developed globular membrane morphology along the long side of the cells that replace the tongue-and-groove interdigitations, and large protrusions along the short side retained the tongue-and-groove interdigitations (Fig. 4A). Nuclear fiber cells had globular membrane morphology (Fig. 4A, panels 6 and 6′) without obvious interlocking protrusions.

In control and *EphA2*$^{-/-}$ lenses, we observed that cortical fiber cells are similar between control and *EphA2*$^{-/-}$ cells, but *EphA2*$^{-/-}$ cortical fibers are more disorganized (Fig. 4B, panels 1-2), consistent with previous reports of misaligned lens fibers.[38,44,67] As the fiber cells continued to mature, *EphA2*$^{-/-}$ fibers had pronounced tongue-and-groove interdigitations (Fig. 4B, panels 3 and insets 3 ′, *star*) with smaller interlocking protrusions (*arrows*), compared those in control cells (*arrowheads*). While maturing control cells had tongue-and-groove interdigitations on the long sides of the cells, their pattern was different from the membrane indentations in *EphA2*$^{-/-}$ cells (Fig. 4B, panels 4 and insets 4′, # and *star*). Perinuclear fibers in the *EphA2*$^{-/-}$ lens retained the prominent tongue-and-groove interdigitations on the long and short sides of the cell with much smaller and pointy interlocking protrusions (Fig. 4B, panels 5 and insets 5′, *star* and *arrows*). Nuclear *EphA2*$^{-/-}$ fibers had only small areas of globular membrane morphology (Fig. 4B, panels 6 and insets 6′, *asterisks*) and retained the tongue-and-groove interdigitations (*pound signs*). The fibers closest to the center of the *EphA2*$^{-/-}$ lens had globular membrane morphology without obvious interlocking protrusions similar to that found in control cells (Fig. 4B, panels 7). These data suggested that EphA2 is required for normal maturation of lens fibers by controlling membrane morphology reorganization. It is possible that these differences in cell membranes also lead to changes in lens nuclear stiffness in *EphA2*$^{-/-}$ lenses.

EphA2 is Expressed in the Epithelial Cells and Cortical Fibers, but is Absent From the Lens Nucleus

The small nuclear phenotype and unusual cell membrane morphologies in *EphA2*$^{-/-}$ lenses suggested the EphA2

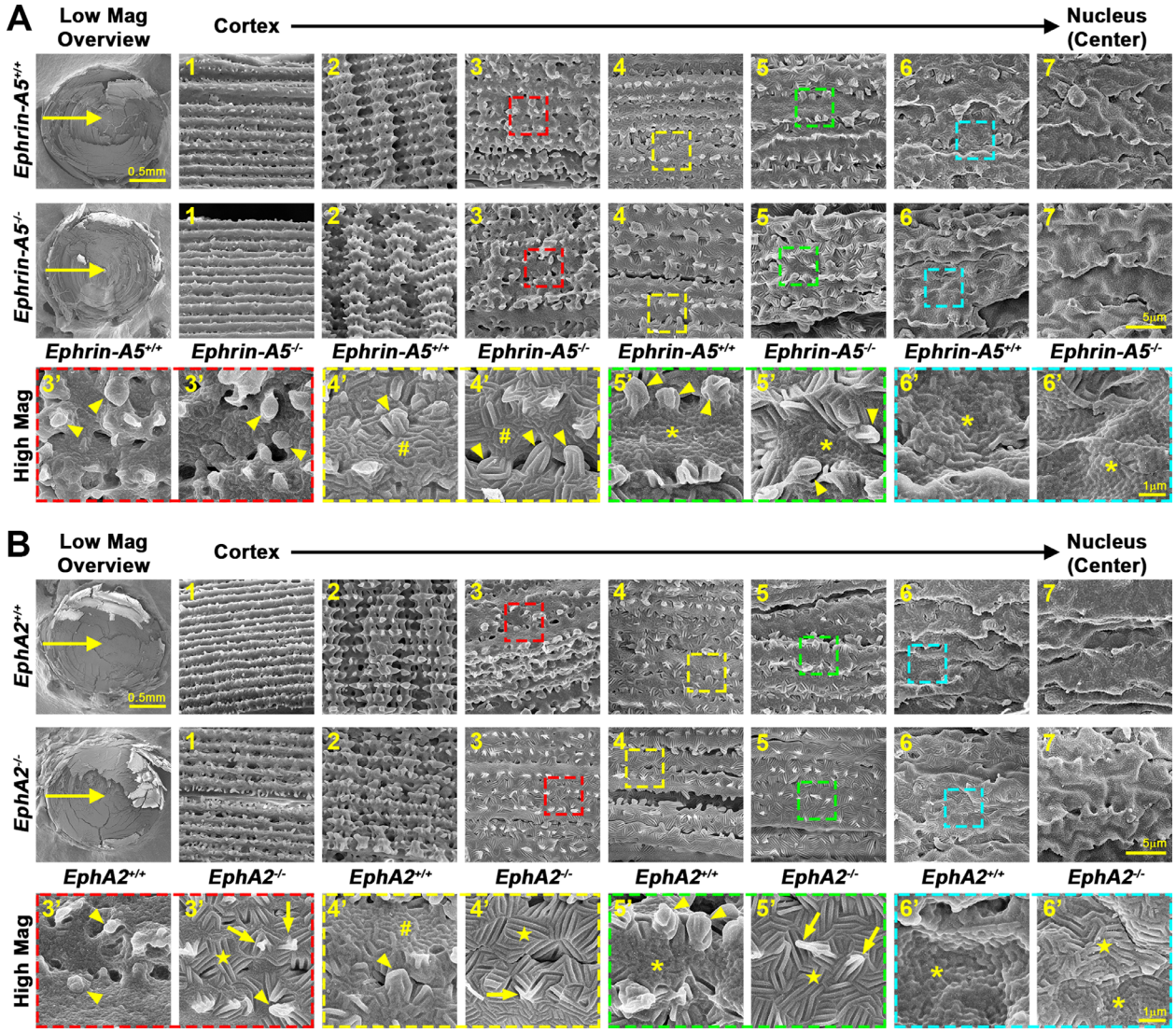

Figure 4. Representative SEM images from 8-week-old control, *ephrin-A5*$^{-/-}$ and *EphA2*$^{-/-}$ lenses taken from cortical fiber cells (*left*) to lens nucleus (*right*). (**A**) Control and *ephrin-A5*$^{-/-}$ lens fibers were comparable at different depths through the lens. The peripheral cortical fibers (panels 1) had flat cells with small protrusions along the short sides. As fibers mature, there are large paddles decorated with small protrusions (panels 2). In maturing fibers, there are large interlocking protrusions along the short sides of the cells (panels 3 and insets 3', *arrowheads*). Maturing fibers develop tongue-and-groove interdigitations in both the long sides of the cell (*pound signs*) and the protrusions (*arrowheads*) along the short sides (panels 4 and insets 4'). Perinuclear fibers (panels 5 and insets 5') have globular membrane morphology (*asterisks*) along the short side of the cell with large protrusions that retain the tongue-and-groove morphology (*arrowheads*). Nuclear fibers (panels 6-7 and insets 6') have globular membrane morphology (*asterisks*). (**B**) Control and *EphA2*$^{-/-}$ cortical lens fibers are similar with small protrusions along the short sides (panels 1). *EphA2*$^{-/-}$ lens fibers have large paddles with small protrusions, but the paddles are misaligned compared to control cells (panels 2). Maturing fibers (panels 3 and insets 3') of the *EphA2*$^{-/-}$ lens have pronounced tongue-and-groove interdigitations (*star*) with a few large protrusion (*arrowhead*) and many smaller and pointy protrusions (*arrows*). In contrast to control cells with normal tongue-and-groove membrane morphology (*pound signs*), *EphA2*$^{-/-}$ maturing fibers (panels 4 and insets 4') have altered tongue-and-groove interdigitations (*star*) with abnormal protrusions (*arrow*). In perinuclear *EphA2*$^{-/-}$ fibers (panels 5 and insets 5'), the cell retain abnormal tongue-and-groove membrane morphology (*star*) compared to normal globular membrane morphology in control cells (*asterisk*). Nuclear *EphA2*$^{-/-}$ fibers (panels 6-7 and insets 6') have delayed transition from tongue-and-groove membrane morphology (*star*) to globular membrane morphology (*asterisk*). *Scale bars*: 1 mm, 5 μm, and 1 μm.

is required for lens nuclear formation. We determined whether the changes in the lens nucleus were due to the loss of EphA2 in the nucleus or whether EphA2 is required only for the maturation programming of cortical fibers before possible nuclear compaction. We performed capillary-electrophoresis–based Western blots of protein lysates from the whole lens, epithelial cells, cortical fibers and nuclear fibers from control, *ephrin-A5*$^{-/-}$ and *EphA2*$^{-/-}$ lenses. In control and *ephrin-A5*$^{-/-}$ lenses, EphA2 was present in the whole lens and epithelial cell and cortical fiber cell fractions but was absent from the lens nucleus (Fig. 5). We showed the pseudo-lane view that is similar to traditional Western blots, as well as representative electropherograms of the actual chemiluminescent peaks detected within capillaries. EphA2 protein level was normalized to the total protein peaks, and there was no significant difference

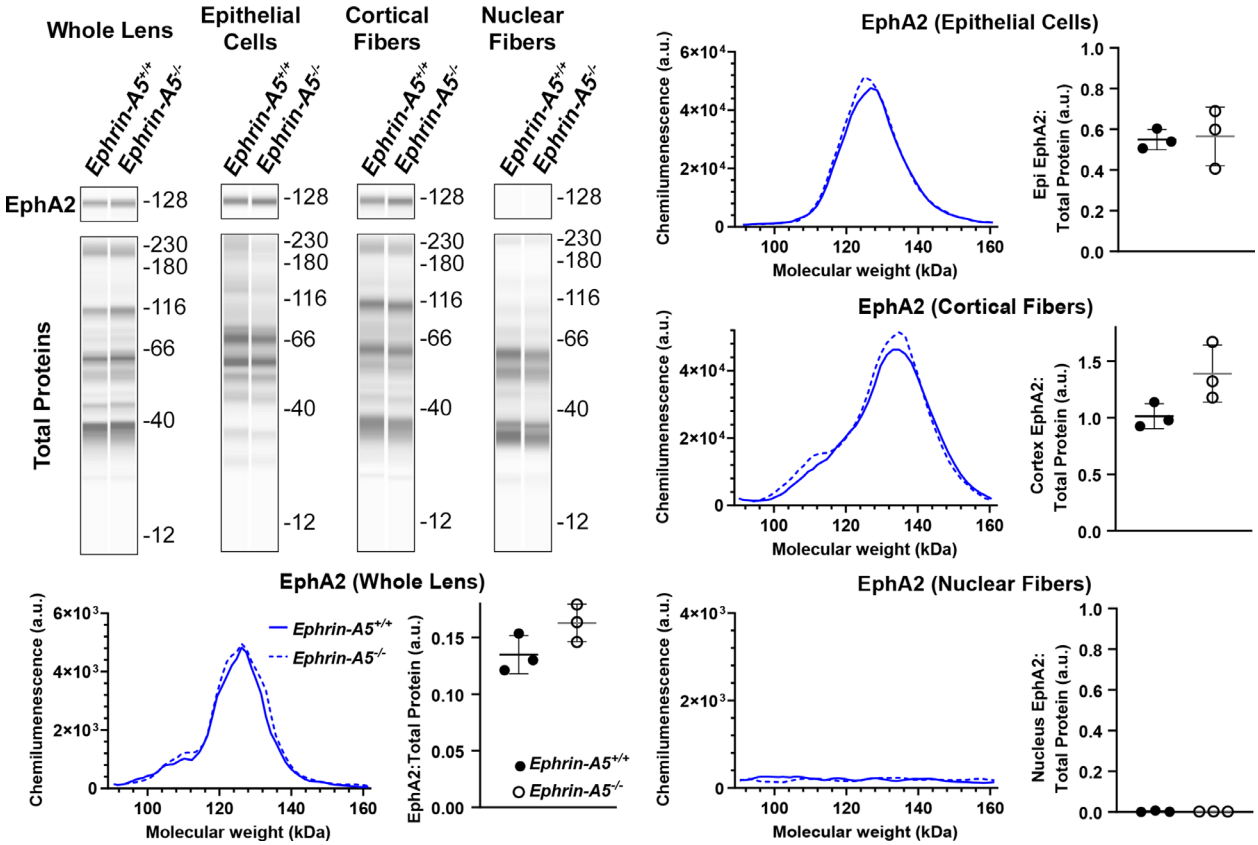

Figure 5. WES capillary-based Westerns demonstrate EphA2 is detected in the whole lens protein sample, lens epithelial cells and cortical fibers, but is not present in nuclear fibers cells of 6-week-old control and *ephrin-A5*$^{-/-}$ lenses. Representative gel bands for EphA2 (~128kDa) and total protein profiles (12–230 kDa) from each fraction and genotype are presented in pseudo-lane views. Representative electropherogram of EphA2 peaks from different fractions is plotted for control and *ephrin-A5*$^{-/-}$ samples. Dot plots show the average and standard deviation of EphA2 amount normalized to the total protein for each fraction. There is no difference detected between control and *ephrin-A5*$^{-/-}$ lenses in the amount of EphA2 in each protein fraction.

in EphA2 protein levels between control and *ephrin-A5*$^{-/-}$ lenses in any of the fractions. Similarly, in *EphA2*$^{+/+}$ lenses, we found the EphA2 was present in the whole lens, epithelial cell and cortical fiber fractions, but absent from nuclear fibers (Fig. 6). *EphA2*$^{-/-}$ samples with no signal indicated that this antibody is specific for EphA2. When we measured the total protein concentration using the Bradford assay after sample homogenization (data not shown) and when we compared the total protein peak profiles, each fraction of the control and KO lens samples were comparable, and we did not observe missing bands/peaks in the total protein peaks of KO samples, indicating that there were no large changes in protein levels in KO lenses. Thus these results suggested that EphA2 likely plays a role in the maturation programming of lens fibers to affect fiber cell interdigitations as cells age and become closer to the lens nucleus.

Discussion

Our results show that EphA2 and ephrin-A5 disruption can alter the shape of the lens and that loss of EphA2 leads to abnormal lens nuclear size and possible changes in stiffness (Fig. 7). The change in lens shape is quite subtle, with *ephrin-A5*$^{-/-}$ and *EphA2*$^{-/-}$ lenses being slightly more spherical than control lenses. Len shape changes could be a result of abnormalities in suture formation in these KO lenses that have been observed recently[68] and in *EphA2*$^{-/-}$ lenses in a previous study.[37] More sophisticated 3D modeling is needed to understand whether and/or how suture patterning and fiber cell elongation alterations contribute to the lens shape and lead to any alterations in KO lenses. We have shown that EphA2 plays a crucial role in the size and possibly the stiffness of the lens nucleus, and this may be the mechanism for mild nuclear cataracts that were observed previously in *EphA2*$^{-/-}$ lenses.[38,67] The changes in the nucleus may be linked to the membrane interdigitations of maturing fiber cells. Although previous works have hypothesized that increase nuclear stiffness leads to increased whole lens stiffness with age,[5,30,32] the mechanisms for nuclear fiber compaction in mammalian lenses and the subsequent increase in stiffness remained unclear. Our data show that EphA2 is required for a series of remodeling and cell morphology changes that occur in fiber cell membranes during a complex maturation process that eventually leads to a very protein-dense, stiff lens nucleus with a relatively high refractive index. This may be caused by cell compaction or an increase in protein density by other, yet unknown, means. Consistent with previous reports,[33,37] EphA2 is not present in the lens nucleus, and, hence, whether this protein acts on the nuclear fiber cell membranes to affect their organization

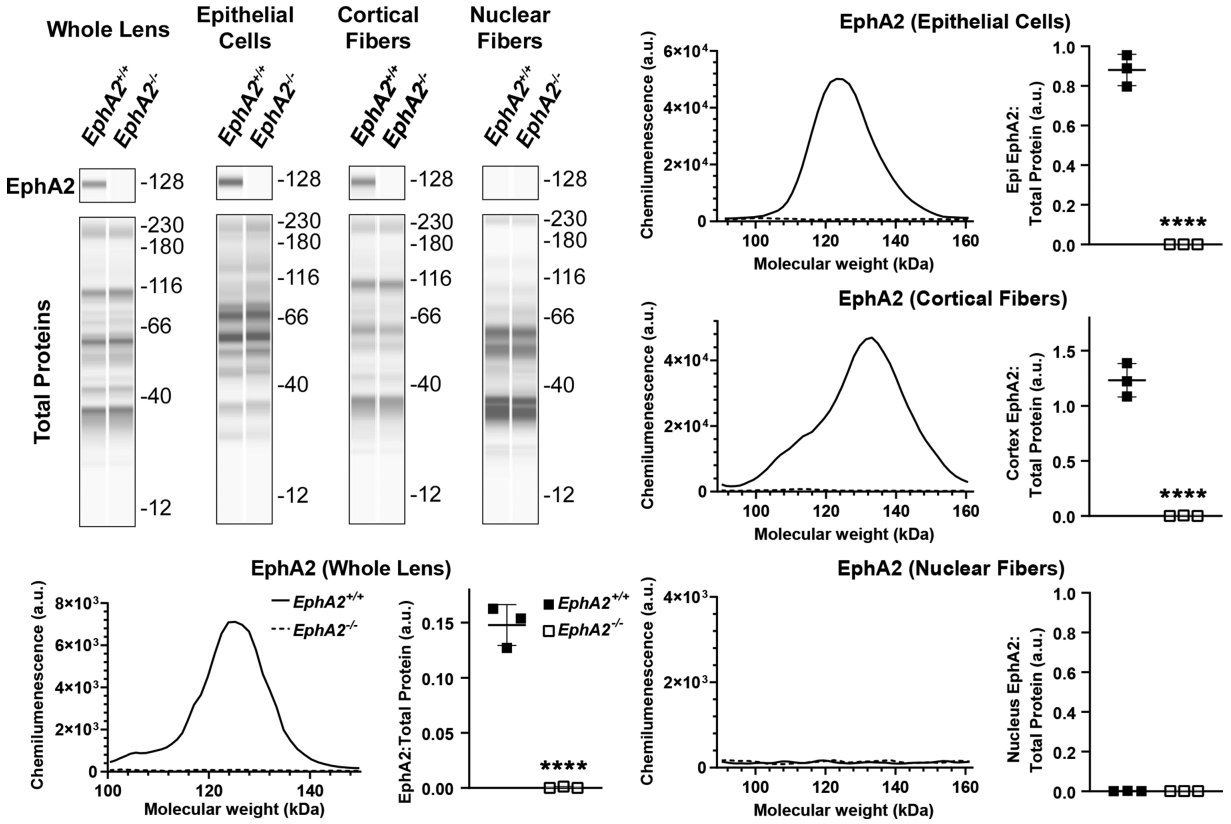

Figure 6. WES capillary-based Westerns demonstrate EphA2 is detected in the whole lens protein sample, lens epithelial cells and cortical fibers, but is not present in nuclear fibers cells of 6-week-old control lenses. Absence of signal in *EphA2*$^{-/-}$ samples confirms the specificity of the antibody. Representative gel bands for EphA2 (~128kDa) and total protein profiles (12–230 kDa) from each fraction and genotype are presented in pseudo-lane views. Representative electropherogram of EphA2 peaks from different fractions is plotted for control and *EphA2*$^{-/-}$ samples. Dot plots show the average and standard deviation of EphA2 amount normalized to the total protein for each fraction. ****, $P < 0.0001$.

or whether the organization is a manifestation of the lack of EphA2 requires further investigation. More sophisticated biomechanical testing will be needed to quantify the change in stiffness in *EphA2*$^{-/-}$ nuclei.

Eph-ephrin signaling is known to trigger a variety of downstream pathways, including Ras/Rho, MAP kinase, Akt and FAK, that affect cytoskeletal structures and cell-cell contact (reviewed in[49,52,69]). It is not clear what downstream pathways are activated by EphA2 signaling that may affect lens fiber cell morphology. Previous investigations have described the presence of interlocking protrusions, tongue-and-groove interdigitations and globular membrane morphology in deep cortical perinuclear and nuclear lens fibers,[70-79] but little is known about how these membrane specializations form and the mechanisms that drive the change in membrane morphology as the cells mature. This work suggests that EphA2 plays a role in the changes in cell interdigitations that take place as fiber cells mature beyond areas where cells have large paddles decorated with small protrusions. In the absence of EphA2, the maturing fiber cells near the lens nucleus fail to undergo the changes in membrane morphology that occur in the control lenses. Our previous work has shown that fiber cell morphology may be linked to lens stiffness, and large paddles in the maturing fibers may be required to maintain lens stiffness at low compressive forces.[62] Therefore it is possible that globular membrane morphology of nuclear fiber cells also contributes to the stiffness of those cells. Further immunofluorescence and biochemical studies of the differences between inner and perinuclear fibers from control and *EphA2*$^{-/-}$ lenses is needed to provide further insights into the mechanism for the fiber cell maturation and possible nuclear fiber cell compaction.

Our previous work demonstrated that *ephrin-A5*$^{-/-}$ lenses sometimes develop anterior cataracts due to epithelial-to-mesenchymal transition in normally quiescent anterior lens epithelial cells.[38,67] Consistent with those works, our current results reveal that *ephrin-A5*$^{-/-}$ lenses had normal lens fiber cell morphology when compared to controls. The mice used for this study and in our previous work are mostly in the C57BL6 background. In contrast to the relatively mild lens phenotype in our C57BL6 *ephrin-A5*$^{-/-}$ mice, *ephrin-A5*$^{-/-}$ mice in a mixed 129/SV/C57BL6 background have severe cataracts with lens rupture.[35,80,81] Mixed background *ephrin-A5*$^{-/-}$ lenses had degenerated fiber cells with abnormal membrane morphology.[35,80,81] The variable lens phenotypes of different strains of *ephrin-A5*$^{-/-}$ mice suggest that genetic modifiers affect cataract severity and determine whether defects are present in epithelial or fiber cells.

The smaller and softer lens nucleus correlates with the decrease in refractive index magnitude across the nucleus of *EphA2*$^{-/-}$ lenses. Previous studies have suggested that high protein concentration in the lens nucleus[82-84] or compaction

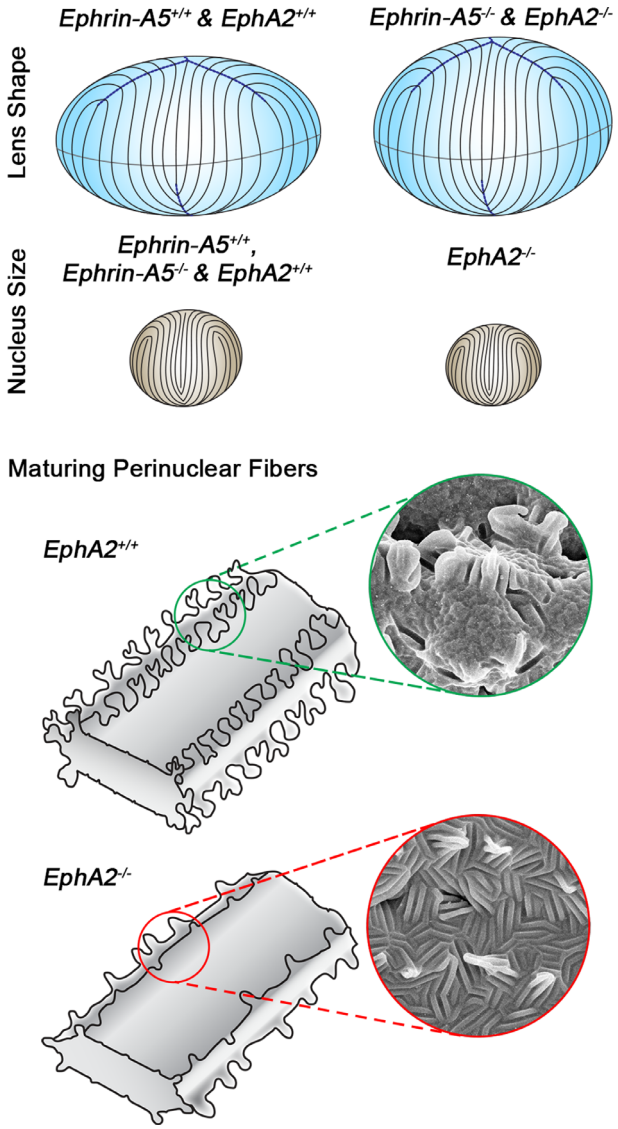

Figure 7. Compared to controls, *ephrin-A5*$^{-/-}$ and *EphA2*$^{-/-}$ lenses are more spherical in shape, and *EphA2*$^{-/-}$ lenses have smaller and softer lens nuclei. The smaller lens nuclei in *EphA2*$^{-/-}$ lenses are correlated with membrane interdigitation changes in perinuclear fiber cells. Perinuclear control fibers have large interlocking protrusions along the short sides of the fiber cells that have tongue-and-groove interdigitations whereas the long sides of the cells have globular membrane morphology. In contrast, *EphA2*$^{-/-}$ perinuclear lens fibers have small and pointy protrusions, and the entire cell membrane displays deep and abnormal tongue-and-groove interdigitations. Images not drawn to scale.

of the nuclear fibers[5,6,85] results in high refractive index at the center of the lens.[29] Our work in aging mouse lenses suggested that the increased area of high refractive index in lenses from old mice is correlated with the increase in size of the hard, compact lens nucleus.[29] This work indicates that in mouse lenses, high refractive index may be related to the compaction of the lens nucleus since the smaller and softer lens nuclei of *EphA2*$^{-/-}$ lenses is directly correlated with a smaller area of high refractive index with a significantly lower maximum refractive index. To better understand the impact of compaction on GRIN, more detailed analysis of nuclear fiber size and density in the compact region and comparison between lenses from young and old mice will be needed to reveal whether compaction drives the increase in GRIN in mouse lenses. From our total protein profiles, there were no obvious changes in the main protein peaks, including crystallins, between control and *EphA2*$^{-/-}$ lens homogenates in the whole lens or subfractions of the lens (Fig. 6). Thus it is unlikely that the significant refractive index changes seen in *EphA2*$^{-/-}$ lenses are caused by changes in overall protein levels. We will need to further analyze the protein profile of control and *EphA2*$^{-/-}$ lens nuclei to determine whether there are subtle biochemical changes that may contribute to the decreased refractive index at the center of *EphA2*$^{-/-}$ lenses.

In *ephrin-A5*$^{-/-}$ lenses, the overall GRIN profile is similar to control lenses, but there is a small, but significant, decrease in the maximum refractive index at the center of the *ephrin-A5*$^{-/-}$ nucleus. Thus, the nucleus of the *ephrin-A5*$^{-/-}$ lenses is mostly normal, but there may be a subtle developmental change in the central region resulting in the lower maximum refractive index compared to control lenses. The total protein profile of the control lens nucleus is comparable to that of the nucleus in *ephrin-A5*$^{-/-}$ lenses suggesting no alteration in total protein content in these lenses. Since little is known about nuclear formation, studies of embryonic *ephrin-A5*$^{-/-}$ lenses are needed to elucidate the mechanism for the development the GRIN in mouse lenses and why there may be a difference in maximum refractive index in the control and *ephrin-A5*$^{-/-}$ lenses.

In human lenses, it has long been hypothesized the nucleus stiffness and size affect the overall biomechanical properties of the lens, and that increased nucleus size and stiffness contributes to the development of presbyopia.[5,30,32] Data from this study and from a recent biomechanical investigation of *EphA2*$^{-/-}$ lenses[68] show that, in mice, whole lens stiffness is not directly influenced by the size or stiffness of the lens nucleus because the overall lens stiffness is also affected by the size and stiffness of the cortex. These findings are supported by our previous work showing that mouse lenses with an actin-binding protein deficiency were softer than controls despite an enlarged and stiff nucleus in the knockdown lenses.[61] In lenses from very old mice, the enlarged lens nucleus does not proportionally affect overall lens stiffness.[29] It is important to conduct more thorough investigations on the biomechanical properties of the lens cortex and nucleus taking into account the variations in protein distribution that create the refractive index gradient[85] to build a detailed model of the whole lens to understand the relative contributions of peripheral and nuclear fibers to the stiffness and resilience of the lens. Further studies to examine *EphA2*$^{-/-}$ lenses from old mice are needed to determine whether the nuclear size remains small due to disruption of Eph-ephrin signaling and to measure the whole lens and nuclear stiffness as well as the GRIN. Given that protein density determines the magnitude of refractive index, development of this critical optical property may yield further understanding of the opto-mechanical relationship of the mouse lens and the contribution of nuclear size and stiffness to whole lens functional properties. As compaction is not found in all species, comparison of lenses from young and old animals from a range of accommodating and non-accommodating lenses may provide more information about the mechanism of development of the GRIN and the biomechanical properties in any given species.

Investigative Ophthalmology & Visual Science

Acknowledgments

The authors thank Theresa Fassel and Kimberly Vanderpool at the Scripps Research Core Microscopy Facility for their expert advice and assistance with sample preparation and collection of electron microscope images. We thank Subashree Murugan and Michael Vu for technical assistance and Justin Parreno for his critical reading of the manuscript and helpful discussion.

Supported by grant R01 EY032056 (to CC) from the National Eye Institute, beamtime grants 2018A1105 and 2019A1115 (to BP and KW) from SPring-8 synchrotron (Japan) and grant 82000878 from National Natural Science Foundation of China.

Disclosure: **C. Cheng,** None; **K. Wang,** None; **M. Hoshino,** None; **K. Uesugi,** None; **N. Yagi,** None; **B. Pierscionek,** None

References

1. Piatigorsky J. Lens differentiation in vertebrates. A review of cellular and molecular features. *Differentiation*. 1981;19:134–153.
2. Bassnett S, Winzenburger PA. Morphometric analysis of fibre cell growth in the developing chicken lens. *Exp Eye Res*. 2003;76:291–302.
3. Kuszak JR. The ultrastructure of epithelial and fiber cells in the crystalline lens. *Int Rev Cytol*. 1995;163:305–350.
4. Bassnett S. Lens organelle degradation. *Exp Eye Res*. 2002;74:1–6.
5. Heys KR, Cram SL, Truscott RJ. Massive increase in the stiffness of the human lens nucleus with age: the basis for presbyopia? *Molecular vision*. 2004;10:956–963.
6. Al-Ghoul KJ, Nordgren RK, Kuszak AJ, Freel CD, Costello MJ, Kuszak JR. Structural evidence of human nuclear fiber compaction as a function of ageing and cataractogenesis. *Exp Eye Res*. 2001;72:199–214.
7. Wang K, Hoshino M, Uesugi K, et al. Cell compaction is not required for the development of gradient refractive index profiles in the embryonic chick lens. *Exp Eye Res*. 2020;197:108112.
8. Kozlowski TM, Kroger RHH. Constant lens fiber cell thickness in fish suggests crystallin transport to denucleated cells. *Vis Res*. 2019;162:29–34.
9. Glasser A, Campbell MC. Biometric, optical and physical changes in the isolated human crystalline lens with age in relation to presbyopia. *Vis Res*. 1999;39:1991–2015.
10. Weeber HA, Eckert G, Soergel F, Meyer CH, Pechhold W, van der Heijde RG. Dynamic mechanical properties of human lenses. *Exp Eye Res*. 2005;80:425–434.
11. Heys KR, Friedrich MG, Truscott RJ. Presbyopia and heat: changes associated with aging of the human lens suggest a functional role for the small heat shock protein, alpha-crystallin, in maintaining lens flexibility. *Aging Cell*. 2007;6:807–815.
12. Pierscionek BK. Age-related response of human lenses to stretching forces. *Exp Eye Res*. 1995;60:325–332.
13. Weeber HA, van der Heijde RG. On the relationship between lens stiffness and accommodative amplitude. *Exp Eye Res*. 2007;85:602–607.
14. Fisher RF. Elastic properties of the human lens. *Exp Eye Res*. 1971;11:143.
15. Krueger RR, Sun XK, Stroh J, Myers R. Experimental increase in accommodative potential after neodymium: yttrium-aluminum-garnet laser photodisruption of paired cadaver lenses. *Ophthalmology*. 2001;108:2122–2129.
16. Burd HJ, Wilde GS, Judge SJ. An improved spinning lens test to determine the stiffness of the human lens. *Exp Eye Res*. 2011;92:28–39.
17. Glasser A, Campbell MC. Presbyopia and the optical changes in the human crystalline lens with age. *Vis Res*. 1998;38:209–229.
18. Pau H, Kranz J. The increasing sclerosis of the human lens with age and its relevance to accommodation and presbyopia. *Graefes Arch Clin Exp Ophthalmol*. 1991;229:294–296.
19. Hollman KW, O'Donnell M, Erpelding TN. Mapping elasticity in human lenses using bubble-based acoustic radiation force. *Exp Eye Res*. 2007;85:890–893.
20. Besner S, Scarcelli G, Pineda R, Yun SH. In Vivo Brillouin Analysis of the Aging Crystalline Lens. *Invest Ophthalmol Vis Sci*. 2016;57:5093–5100.
21. Sharma PK, Busscher HJ, Terwee T, Koopmans SA, van Kooten TG. A comparative study on the viscoelastic properties of human and animal lenses. *Exp Eye Res*. 2011;93:681–688.
22. Zhang X, Wang Q, Lyu Z, et al. Noninvasive assessment of age-related stiffness of crystalline lenses in a rabbit model using ultrasound elastography. *Biomed Eng Online*. 2018;17:75.
23. Wu C, Han Z, Wang S, et al. Assessing age-related changes in the biomechanical properties of rabbit lens using a coaligned ultrasound and optical coherence elastography system. *Invest Ophthalmol Vis Sci*. 2015;56:1292–1300.
24. Baradia H, Nikahd N, Glasser A. Mouse lens stiffness measurements. *Exp Eye Res*. 2010;91:300–307.
25. Gokhin DS, Nowak RB, Kim NE, et al. Tmod1 and CP49 synergize to control the fiber cell geometry, transparency, and mechanical stiffness of the mouse lens. *PloS One*. 2012;7:e48734.
26. Sindhu Kumari S, Gupta N, Shiels A, et al. Role of Aquaporin 0 in lens biomechanics. *Biochem Biophys Res Commun*. 2015;462:339–345.
27. Fudge DS, McCuaig JV, Van Stralen S, et al. Intermediate filaments regulate tissue size and stiffness in the murine lens. *Invest Ophthalmol Vis Sci*. 2011;52:3860–3867.
28. Cheng C, Gokhin DS, Nowak RB, Fowler VM. Sequential application of glass coverslips to assess the compressive stiffness of the mouse lens: strain and morphometric analyses. *J Vis Exp*. 2016;111:53986.
29. Cheng C, Parreno J, Nowak RB, et al. Age-related changes in eye lens biomechanics, morphology, refractive index and transparency. *Aging*. 2019;11:12497–12531.
30. Weeber HA, Eckert G, Pechhold W, van der Heijde RG. Stiffness gradient in the crystalline lens. *Graefes Arch Clin Exp Ophthalmol*. 2007;245:1357–1366.
31. Heys KR, Truscott RJ. The stiffness of human cataract lenses is a function of both age and the type of cataract. *Exp Eye Res*. 2008;86:701–703.
32. Michael R, Bron AJ. The ageing lens and cataract: a model of normal and pathological ageing. *Philos Trans R Soc Lond B Biol Sci*. 2011;366:1278–1292.
33. Jun G, Guo H, Klein BE, et al. EPHA2 is associated with age-related cortical cataract in mice and humans. *PLoS Genet*. 2009;5:e1000584.
34. Shiels A, Bennett TM, Knopf HL, et al. The EPHA2 gene is associated with cataracts linked to chromosome 1p. *Mol Vis*. 2008;14:2042–2055.
35. Cooper MA, Son AI, Komlos D, Sun Y, Kleiman NJ, Zhou R. Loss of ephrin-A5 function disrupts lens fiber cell packing and leads to cataract. *Proc Natl Acad Sci USA*. 2008;105:16620–16625.
36. Tan W, Hou S, Jiang Z, Hu Z, Yang P, Ye J. Association of EPHA2 polymorphisms and age-related cortical cataract in a Han Chinese population. *Mol Vis*. 2011;17:1553–1558.
37. Shi Y, De Maria A, Bennett T, Shiels A, Bassnett S. A role for epha2 in cell migration and refractive organization of the ocular lens. *Invest Ophthalmol Vis Sci*. 2012;53:551–559.

Investigative Ophthalmology & Visual Science

38. Cheng C, Gong X. Diverse roles of Eph/ephrin signaling in the mouse lens. *PloS one*. 2011;6:e28147.
39. Sundaresan P, Ravindran RD, Vashist P, et al. EPHA2 polymorphisms and age-related cataract in India. *PloS One*. 2012;7:e33001.
40. Masoodi TA, Shammari SA, Al-Muammar MN, Almubrad TM, Alhamdan AA. Screening and structural evaluation of deleterious non-synonymous SNPs of ePHA2 gene involved in susceptibility to cataract formation. *Bioinformation*. 2012;8:562–567.
41. Park JE, Son AI, Hua R, Wang L, Zhang X, Zhou R. Human cataract mutations in EPHA2 SAM domain alter receptor stability and function. *PloS one*. 2012;7:e36564.
42. Kaul H, Riazuddin SA, Shahid M, et al. Autosomal recessive congenital cataract linked to EPHA2 in a consanguineous Pakistani family. *Mol Vis*. 2010;16:511–517.
43. Zhang T, Hua R, Xiao W, et al. Mutations of the EPHA2 receptor tyrosine kinase gene cause autosomal dominant congenital cataract. *Hum Mutat*. 2009;30:E603–611.
44. Cheng C, Ansari MM, Cooper JA, Gong X. EphA2 and Src regulate equatorial cell morphogenesis during lens development. *Development*. 2013;140:4237–4245.
45. Celojevic D, Abramsson A, Seibt Palmer M, et al. EPHA2 Polymorphisms in Estonian Patients with Age-Related Cataract. *Ophthalmic Genet*. 2016;37:14–18.
46. Lin Q, Zhou N, Zhang N, Qi Y. Mutational screening of EFNA5 in Chinese age-related cataract patients. *Ophthalmic Res*. 2014;52:124–129.
47. Berry V, Pontikos N, Albarca-Aguilera M, et al. A recurrent splice-site mutation in EPHA2 causing congenital posterior nuclear cataract. *Ophthalmic Genet*. 2018;39:236–241.
48. Zhai Y, Zhu S, Li J, Yao K. A novel human congenital cataract mutation in EPHA2 kinase domain (p.G668D) alters receptor stability and function. *Invest Ophthalmol Vis Sci*. 2019;60:4717–4726.
49. Kullander K, Klein R. Mechanisms and functions of Eph and ephrin signalling. *Nat Rev Mol Cell Biol*. 2002;3:475–486.
50. Lisabeth EM, Falivelli G, Pasquale EB. Eph receptor signaling and ephrins. *Cold Spring Harb Perspect Biol*. 2013;5(9):a009159.
51. Pasquale EB. Eph-ephrin bidirectional signaling in physiology and disease. *Cell*. 2008;133:38–52.
52. Himanen JP, Saha N, Nikolov DB. Cell-cell signaling via Eph receptors and ephrins. *Curr Opin Cell Biol*. 2007;19:534–542.
53. Davy A, Gale NW, Murray EW, et al. Compartmentalized signaling by GPI-anchored ephrin-A5 requires the Fyn tyrosine kinase to regulate cellular adhesion. *Genes Dev*. 1999;13:3125–3135.
54. Holland SJ, Gale NW, Mbamalu G, Yancopoulos GD, Henkemeyer M, Pawson T. Bidirectional signalling through the EPH-family receptor Nuk and its transmembrane ligands. *Nature*. 1996;383:722–725.
55. Li D, Wang S, Ye H, et al. Distribution of gene mutations in sporadic congenital cataract in a Han Chinese population. *Mol Vis*. 2016;22:589–598.
56. Dave A, Laurie K, Staffieri SE, et al. Mutations in the EPHA2 gene are a major contributor to inherited cataracts in South-Eastern Australia. *PloS one*. 2013;8:e72518.
57. Zhou Y, Shiels A. Epha2 and Efna5 participate in lens cell pattern-formation. *Differentiation*. 2018;102:1–9.
58. Okabe M, Ikawa M, Kominami K, Nakanishi T, Nishimune Y. "Green mice" as a source of ubiquitous green cells. *FEBS Lett*. 1997;407:313–319.
59. Frisen J, Yates PA, McLaughlin T, Friedman GC, O'Leary DD, Barbacid M. Ephrin-A5 (AL-1/RAGS) is essential for proper retinal axon guidance and topographic mapping in the mammalian visual system. *Neuron*. 1998;20:235–243.
60. Blankenship T, Bradshaw L, Shibata B, Fitzgerald P. Structural specializations emerging late in mouse lens fiber cell differentiation. *Invest Ophthalmol Vis Sci*. 2007;48:3269–3276.
61. Cheng C, Nowak RB, Amadeo MB, Biswas SK, Lo WK, Fowler VM. Tropomyosin 3.5 protects the F-actin networks required for tissue biomechanical properties. *J Cell Sci*. 2018;131(23):jcs222042.
62. Cheng C, Nowak RB, Biswas SK, Lo WK, FitzGerald PG, Fowler VM. Tropomodulin 1 regulation of actin is required for the formation of large paddle protrusions between mature lens fiber cells. *Invest Ophthalmol Vis Sci*. 2016;57:4084–4099.
63. Momose A. Recent advances in x-ray phase imaging. *Japanese J Appl Physics*. 2005;44:6355–6367.
64. Momose A, Kawamoto S, Koyama I, Hamaishi Y, Takai K, Suzuki Y. Demonstration of X-Ray Talbot Interferometry. *Japanese J Appl Phys*. 2003;42:L866–L868.
65. Hoshino M, Uesugi K, Yagi N, Mohri S, Regini J, Pierscionek B. Optical properties of in situ eye lenses measured with X-ray Talbot interferometry: a novel measure of growth processes. *PloS One*. 2011;6:e25140.
66. Sugiyama Y, Stump RJ, Nguyen A, et al. Secreted frizzled-related protein disrupts PCP in eye lens fiber cells that have polarised primary cilia. *Dev Biol*. 2010;338:193–201.
67. Cheng C, Fowler VM, Gong X. EphA2 and ephrin-A5 are not a receptor-ligand pair in the ocular lens. *Exp Eye Res*. 2017;162:9–17.
68. Cheng C. EphA2 and Ephrin-A5 guide eye lens suture alignment and influence whole lens resilience. *Invest Ophthalmol Vis Sci*. 2021;62:3.
69. Arvanitis D, Davy A. Eph/ephrin signaling: networks. *Genes Dev*. 2008;22:416–429.
70. Lo WK, Harding CV. Square arrays and their role in ridge formation in human lens fibers. *J Ultrastruct Res*. 1984;86:228–245.
71. Taylor VL, al-Ghoul KJ, Lane CW, Davis VA, Kuszak JR, Costello MJ. Morphology of the normal human lens. *Invest Ophthalmol Vis Sci*. 1996;37:1396–1410.
72. Vrensen GF. Aging of the human eye lens–a morphological point of view. *Comp Biochem Physiol A Physiol*. 1995;111:519–532.
73. Willekens B, Vrensen G. The three-dimensional organization of lens fibers in the rhesus monkey. *Graefes Arch Clin Exp Ophthalmol*. 1982;219:112–120.
74. Kuszak J, Alcala J, Maisel H. The surface morphology of embryonic and adult chick lens-fiber cells. *Am J Anat*. 1980;159:395–410.
75. Willekens B, Vrensen G. The three-dimensional organization of lens fibers in the rabbit. A scanning electron microscopic reinvestigation. *Albrecht Von Graefes Arch Klin Exp Ophthalmol*. 1981;216:275–289.
76. Zhou CJ, Lo WK. Association of clathrin, AP-2 adaptor and actin cytoskeleton with developing interlocking membrane domains of lens fibre cells. *Exp Eye Res*. 2003;77:423–432.
77. Kuszak JR, Macsai MS, Rae JL. Stereo scanning electron microscopy of the crystalline lens. *Scan Electron Microsc*. 1983;1415–1426.
78. Vrensen GF, Duindam HJ. Maturation of fiber membranes in the human eye lens. Ultrastructural and Raman microspectroscopic observations. *Ophthalmic Res*. 1995;27(Suppl 1):78–85.
79. Kuwabara T. The maturation of the lens cell: a morphologic study. *Exp Eye Res*. 1975;20:427–443.
80. Son AI, Cooper MA, Sheleg M, Sun Y, Kleiman NJ, Zhou R. Further analysis of the lens of ephrin-A5$^{-/-}$ mice: development of postnatal defects. *Mol Vis*. 2013;19:254–266.

Investigative Ophthalmology & Visual Science

81. Biswas S, Son A, Yu Q, Zhou R, Lo WK. Breakdown of interlocking domains may contribute to formation of membranous globules and lens opacity in ephrin-A5(-/-) mice. *Exp Eye Res*. 2016;145:130–139.
82. Axelrod D, Lerner D, Sands PJ. Refractive index within the lens of a goldfish eye determined from the paths of thin laser beams. *Vis Res*. 1988;28:57–65.
83. Verma Y, Rao KD, Suresh MK, Patel HS, Gupta PK. Measurement of gradient refractive index profile of crystalline lens of fisheye in vivo using optical coherence tomography. *Appl Phys B*. 2007;87:607–610.
84. Kozlowski TM, Kroger RHH. Visualization of adult fish lens fiber cells. *Exp Eye Res*. 2019;181:1–4.
85. Pierscionek BK, Regini JW. The gradient index lens of the eye: an opto-biological synchrony. *Prog Retin Eye Res*. 2012;31:332–349.

Investigative Ophthalmology & Visual Science